Hindawi
Shock and Vibration
Volume 2019, Article ID 4080274, 13 pages
https://doi.org/10.1155/2019/4080274

Research Article

Blasting Impact Simulation Test and Fragmentation Distribution Characteristics in an Open-Pit Mine

Xiaohua Ding[1,2], **Xiang Lu**[1,2], **Wei Zhou**[1,2], **Xuyang Shi**[1,2], **Boyu Luan**[1,2] and **Ming Li**[3]

[1]*School of Mines, China University of Mining & Technology, Xuzhou, Jiangsu 221116, China*
[2]*State Key Laboratory of Coal Resources and Safe Mining, China University of Mining & Technology, Xuzhou, Jiangsu 221116, China*
[3]*State Key Laboratory for Geomechanics and Deep Underground Engineering, China University of Mining & Technology, Xuzhou, Jiangsu 221116, China*

Correspondence should be addressed to Xiang Lu; 06122383@cumt.edu.cn and Wei Zhou; zhw19820624@163.com

Received 31 March 2019; Accepted 6 May 2019; Published 27 May 2019

Academic Editor: Alvaro Cunha

Based on the split Hopkinson pressure bar (SHPB) test system, dynamic impact tests of coal specimens under different impact pressures were carried out to study the relationship between the impact load and the size of crushed lump coal. Based on the theory of stress wave attenuation, the relationship between the blasting impact load in a single-hole blasting area of a coal seam and the load applied in an impact failure test of a coal specimen in the laboratory was established. According to the characteristics of the fragmentation distribution of the coal specimens destroyed under a laboratory impact load and the requirement of the minimum cost control of coal blasting in an open-pit coal mine, the fragmentation size range was divided into three groups: large-diameter, medium-diameter, and powder particles. Based on this range, the variation rule of the mass percentage of coal fragments with impact pressure was obtained. Established on the evaluation principle of the blasting effect in an open-pit coal mine, a good impact fragmentation effect was obtained. The good pressure range is $0.30\ \text{MPa} \le P < 0.90\ \text{MPa}$.

1. Introduction

The mining industry contributes millions of dollars to the world economy [1–3], where blasting plays an important role. The impact load is the core of laboratory simulations of coal blasting tests [4–9]. The determination of an accurate impact load is the premise of the scientific analysis of the fragmentation distribution of coal blasting [10–13]. The dynamic impact test of coal specimens at different pressures was carried out using a split Hopkinson pressure bar (SHPB) test system. The relationship between the impact load and the size of fragmented lump coal was studied, which provided an important scientific basis for optimizing the blasting parameters of open-pit coal seams.

According to the degree of coal damage after coal seam blasting, the blasting area of a single hole can be divided. As shown in Figure 1, each damage area is simplified into a spherical space, and the damage areas are the blasting core area, powder area, fragment area, crack area, and undisturbed area from the inside to the outside. With the explosive as the center, the degree of coal damage in each region decreases gradually; that is, the scale of coal block damage increases gradually [14–18].

The calculation formula of the blasting shock wave is as follows [19–21]:

$$\Delta P = \eta K \left(\frac{Q^{1/3}}{R} \right)^{\alpha}, \tag{1}$$

where α and K are the empirical coefficients, 1.31 and 0.67, respectively; η is the attenuation index, 0.49; Q is the charge quantity, kg; and R is the distance from a certain point in the coal seam to the explosive center, m.

According to formula (1), assuming that the charge is 1 kg and the radius of the explosive is 0.1 m, the curve of the stress wave with distance R can be obtained. As shown in Figure 2, with increasing distance, the impact load of the

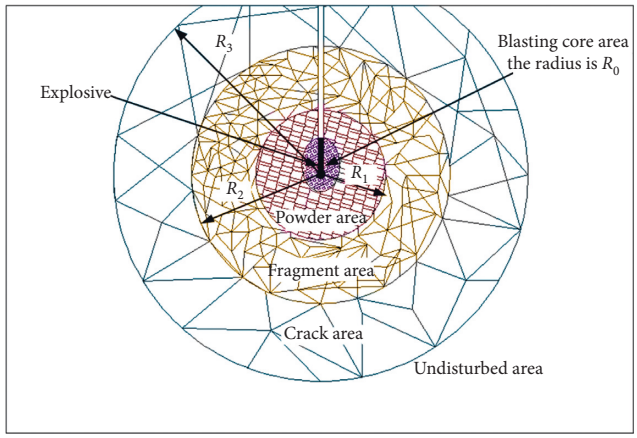

Figure 1: Division of the single-hole area in the coal seam blasting in the open-pit coal mine.

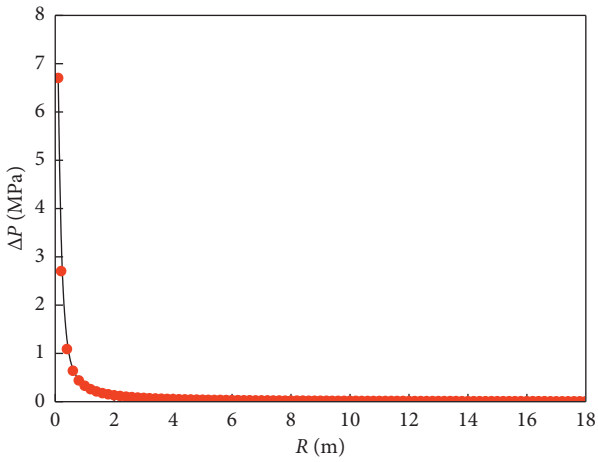

Figure 2: Attenuation characteristics of the blasting impact load with distance R.

impact blasting decreases rapidly, and the attenuation characteristics are obvious.

After the explosion, the stress waves acting on the same sphere are the same at all points. Therefore, the test stress can be determined directly according to formula (1).

To establish the relationship between the laboratory impact tests and coal seam blasting, the conclusions of laboratory tests can be applied to the optimization of blasting engineering in open-pit coal mines. The specific steps are as follows:

(1) Using the design parameters of blasting engineering, according to formula (1), the impact load range of coal around the blasting hole is obtained, and the impact load applied in laboratory tests is determined.

(2) The load at the boundary between the crack area and the undisturbed area is determined by multiple blasting tests; that is, the minimum load of the coal failure can be deduced, and then the maximum radius R3 of the crack area can be deduced.

(3) The mechanical tests of coal specimens under multiple impact loads are designed and the characteristics of coal specimens' failure and fragmentation distribution under different impact loads are analyzed.

(4) Comparing the experimental results of the dynamic characteristics of coal specimens in the laboratory with the results of fragmentation analysis of coal seam blasting in an open-pit coal mine, the range of each fragmentation area of the blasting hole is determined, and finally, the parameter optimization scheme of coal seam blasting is given.

2. Materials and Methods

2.1. Specimen Collection and Preparation. The coal specimens used in this test are from the Haerwusu open-pit coal mine (shown in Figure 3). According to the test plan, the specimens are machined into a cylinder with diameters of 50 mm and heights of 50 mm. To prevent the specimens from peeling off during the experiment, a layer of thermal shrinkage film is wrapped on the surface of the specimen, as shown in Figure 4.

2.2. Instruments and Equipment. This test adopts the instrument $\varphi = 50$ mm SHPB test system [22–24], which belongs to the State Key Laboratory for Geomechanics & Deep Underground Engineering, China University of Mining and Technology. The system consists of five parts: the loading drive system, pressure bar system, energy absorption system, signal acquisition system, and signal processing system. The specimen is sandwiched between the incident rod and the transmission rod.

The loading driving system is the power source and stress wave generating system of the whole system, including a high-pressure gas tank, a pressure gauge, and an impact rod. The high-pressure gas used in this test is ordinary liquid nitrogen, and the pressure gauge is a magnetically electric-contact pressure gauge. The maximum pressure can be selected to be 2.5 MPa, which meets the test requirements. The punch material is 40Cr alloy steel with a diameter of 37 mm and a length of 300 mm. The ultimate strength of the punch is greater than 800 MPa.

The pressure bar system is a fixed support structure for the stress wave propagation medium and specimen, including the incident bar and transmission bar, as shown in Figure 5. In this test system, the material properties of the bar are the same as those of the punch. The length of the incident rod is 2400 mm, and the diameter of the contact end with the impact rod is 37 mm. The diameter of the incident rod changes to 50 mm after passing through the transition section of 600 mm. The transmission rod is 1400 mm in length and 50 mm in diameter.

The energy absorption system is an absorption device of a residual stress wave in a transmission rod, which includes an absorption rod and buffer.

The data acquisition system of this test adopts the two-channel DH5960 ultradynamic signal acquisition instrument produced by Donghua Testing Technology Co., Ltd., Jiangsu Province, China. As shown in Figure 6, the

Figure 3: Collected samples in the mine.

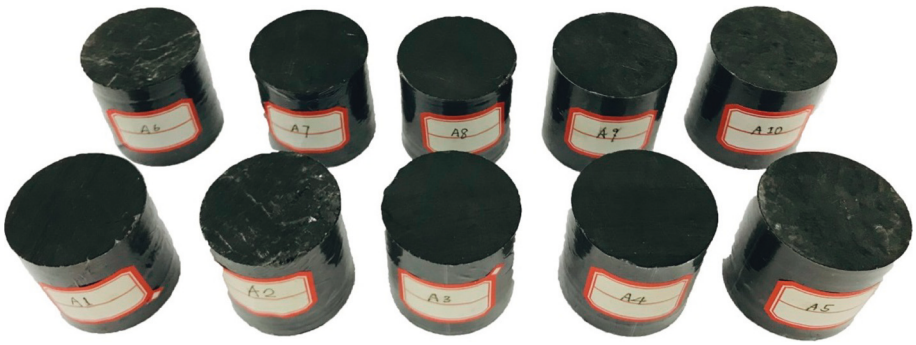

Figure 4: Processed coal specimens.

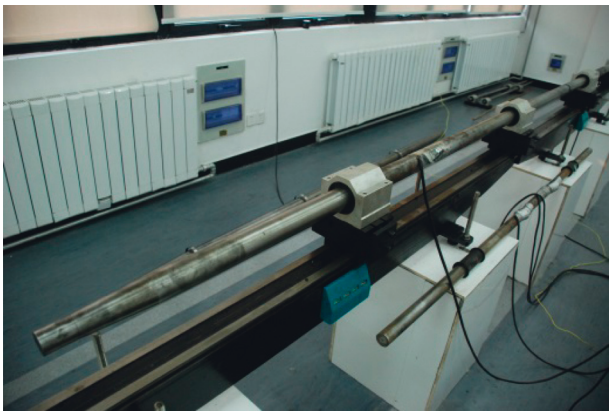

Figure 5: Pressure bar system.

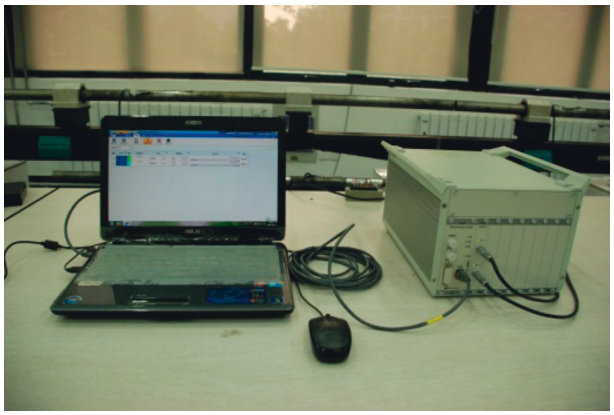

Figure 6: Data acquisition system.

maximum sampling frequency of this system reaches 10 M, which meets the requirements of the signal data acquisition.

The signals of the incident wave, reflected wave, and transmitted wave are obtained by a data acquisition system. To obtain the mechanical properties of rock specimens, two data processing processes are needed:

(1) Filtering the original signal to remove noise

(2) Calculating the dynamic characteristics of the rock specimens

To observe the failure process of the coal specimens under different impact pressures during the experiment, a high-speed camera system (Phantom v611) is used to capture the failure process of the coal specimens under uniaxial compression at different pressures, and the surface crack growth and propagation process are obtained at different times.

2.3. Test Method. During the test, the impact rod collides with the incident rod driven by high-pressure gas and forms an incident pulse in the incident rod. The incident pulse propagates through the incident rod to both sides of the specimen, and the stress pulse acts on the specimen and reflects and transmits multiple times at both ends of the specimen-rod interface, resulting in the high-speed deformation of the specimen. At the same time, one part of the pulse is reflected, and the other part of the pulse is transmitted to the transmission rod through the coal specimen, forming the reflected pulse signal and the transmission pulse signal, respectively. Through the strain gauge on the elastic compression bar, each signal is recorded in the signal acquisition system, and the entire failure process of the specimen is recorded by using the high-speed camera system.

The minimum loading pressure is 0.13 MPa, which indicates that the pressure at the junction of the crack zone and the undisturbed zone is 0.13 The SHPB test system used in this test has a maximum loading pressure of 2.0 MPa. Therefore, the impact load is designed with 0.13 MPa and 2.0 MPa as upper and lower loads. Through many tests, 10 groups of impact tests were designed. The impact loads were 0.13 MPa, 0.17 MPa, 0.25 MPa, 0.30 MPa, 0.50 MPa, 0.70 MPa, 0.90 MPa, 1.20 MPa, 1.50 MPa, and 2.0 MPa.

3. Tests and Discussion

3.1. Impact Tests of the Coal Specimens. The failure process of the coal specimens under impact loading is captured by using a high-speed video camera system, and the failure process of specimens at different times is obtained, as shown in Figure 7. It can be seen from the figure that the failure time interval of the specimen under the impact load is in milliseconds, and the coal specimen is completely destroyed within 3 ms.

3.2. Dynamic Failure Morphological Characteristics of the Coal Specimens. The morphological characteristics of the fragments after failure of the coal specimens under different impact pressures are shown in Figure 8. From the figure, the impact pressure has a significant impact on the morphological characteristics of the fragments after the coal specimen is destroyed. Under lower impact pressure, the damage degree of the specimens is small, and the main fragments after failure are the large volume fragments of the splitting rectangular section (as shown in Figure 9(b)), and the tensile failure characteristics are remarkable. With increasing impact pressure, the number of small fragments increases gradually and the degree of damage increases. From the impact pressure of 0.30 MPa, the small volume fragments increase after the specimen is destroyed, and the fragments are mainly conical-section fragments ((c) in Figure 9) and wedge-section fragments ((d) in Figure 9). The shear fracture surface appears locally. With increasing impact pressure, the proportion of fragments in the conical section and wedge section increases, and the shear fracture surface of the coal specimen under compression increases gradually. It can be inferred that with increasing impact pressure, the failure mode of the coal gradually transforms from tension failure to shear failure. The description of the macrofracture morphology of the coal specimens is only from a qualitative viewpoint; however, the description of the change law of the failure characteristics of coal specimens is from a quantitative viewpoint.

3.3. Distribution Characteristics of Impact Failure Fragments of the Coal Specimens. The fragmentation distribution characteristics of the coal specimens are analyzed by the direct sieving method. The sieves selected in this experiment (as shown in Figure 10) are 15.0 mm, 10.0 mm, 5.0 mm, 2.0 mm, and 1.0 mm in diameter. The specimens are divided into 6 groups of particle sizes: $d = 15.0$ to 50.0 mm, 10.0 to 15.0 mm, 5.0 to 10.0 mm, 2.0 to 5.0 mm, 1.0 to 2.0 mm, and 0.0 to 1.0 mm. Among these groups, 50 mm is the size of the complete coal specimen, and the 6 groups are numbered $i = 1, 2, 3, \ldots, 6$ according to the particle sizes. The coal specimen fragments under different pressure impacts are sieved by grading sieves, and the quality of each grading fragment is obtained, as shown in Figure 11. The first row in each graph corresponds to grading $i = 1$ to 3 from left to right, and the second row corresponds to grading $i = 4$ to 6 from left to right. Overall, with an increase in the impact pressure, the size of large particles decreases and the size of small particles increases. It can be inferred that the degree of coal fragmentation increases with increasing impact pressure.

After sieving, the mass percentage is taken as the fragmentation distribution parameter, that is, the percentage of the mass of the fragments of each size group to the mass of the original coal specimen. To show the damage degree of coal specimens under different impact loads, the average particle size of the fragments is used as the evaluation index in this test. The specific acquisition methods of the index are as follows: first, the fragments are sieved by grading sieves and the mass of each group of particle size fragments (m_{di}) is obtained by a high-precision electronic scale. Second, the mass percentage of each group of the particle size fragments

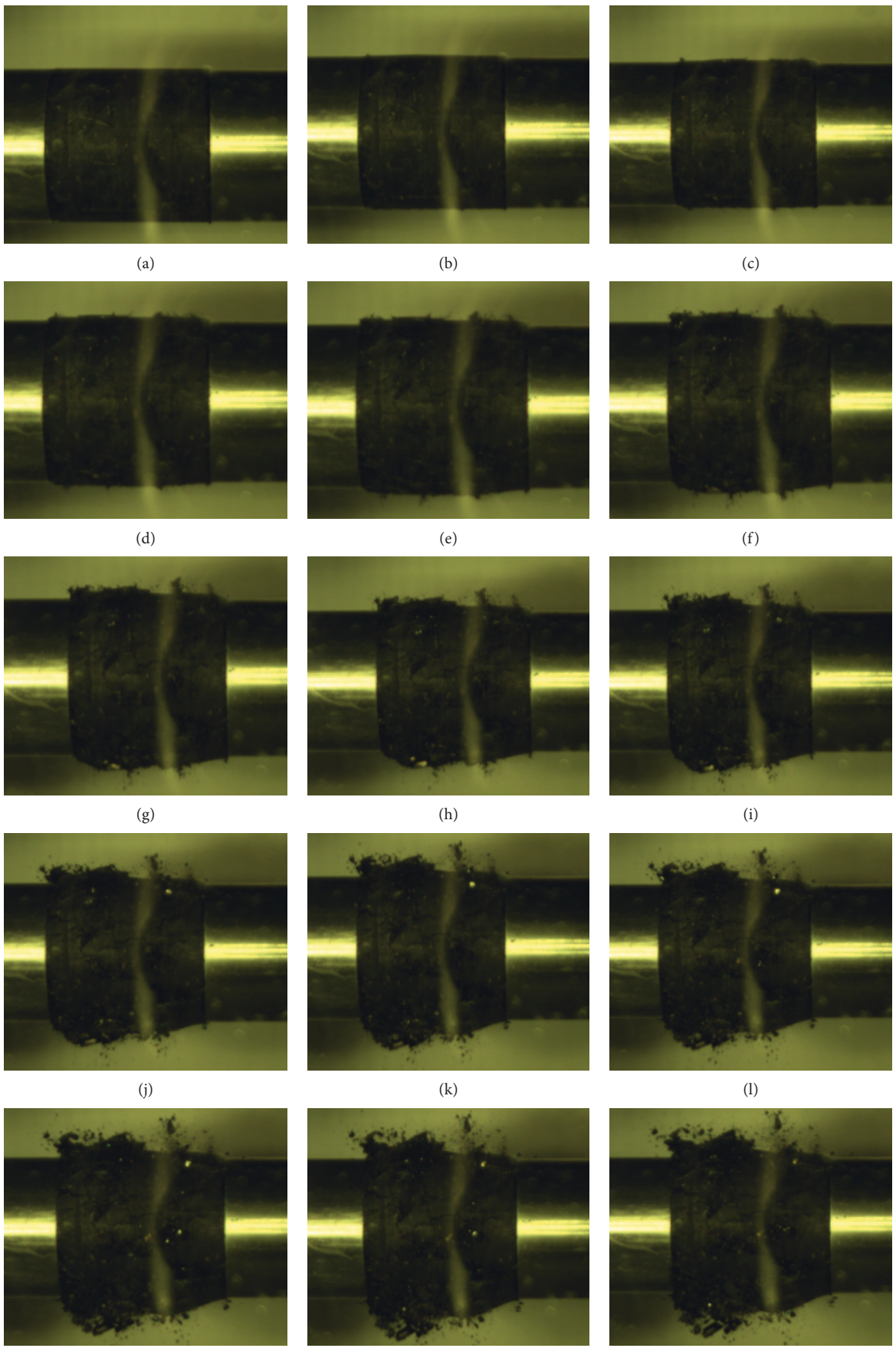

(a) (b) (c)

(d) (e) (f)

(g) (h) (i)

(j) (k) (l)

(m) (n) (o)

Figure 7: Continued.

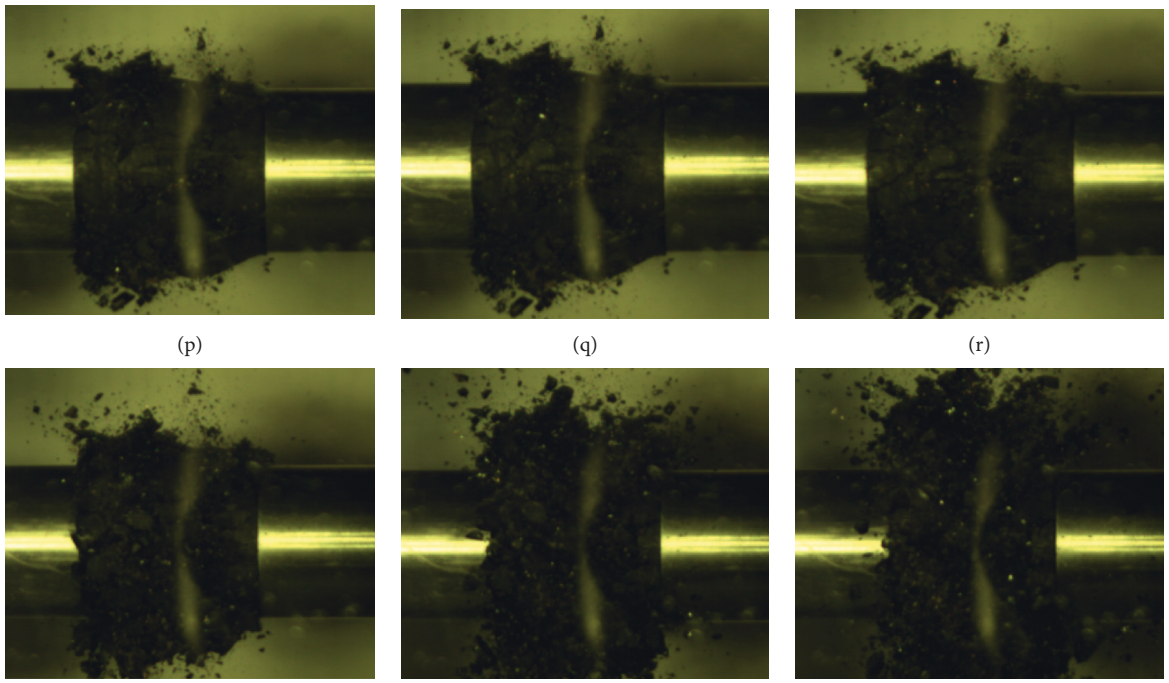

Figure 7: Failure process of the coal specimens under the impact load. (a) $t = 0$ ms. (b) $t = 0.07$ ms. (c) $t = 0.14$ ms. (d) $t = 0.21$ ms. (e) $t = 0.28$ ms. (f) $t = 0.35$ ms. (g) $t = 0.42$ ms. (h) $t = 0.50$ ms. (i) $t = 0.57$ ms. (j) $t = 0.64$ ms. (k) $t = 0.71$ ms. (l) $t = 0.78$ ms. (m) $t = 0.85$ ms. (n) $t = 0.92$ ms. (o) $t = 1.00$ ms. (p) $t = 1.07$ ms. (q) $t = 1.14$ ms. (r) $t = 1.21$ ms. (s) $t = 1.78$ ms. (t) $t = 2.36$ ms. (u) $t = 2.86$ ms.

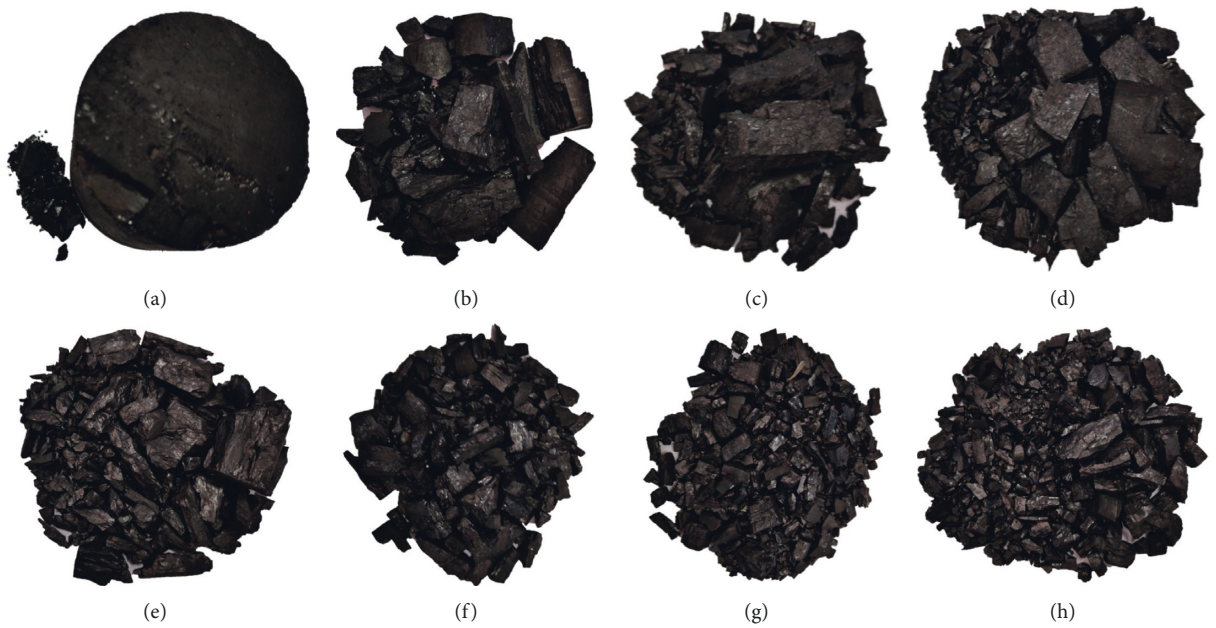

Figure 8: Continued.

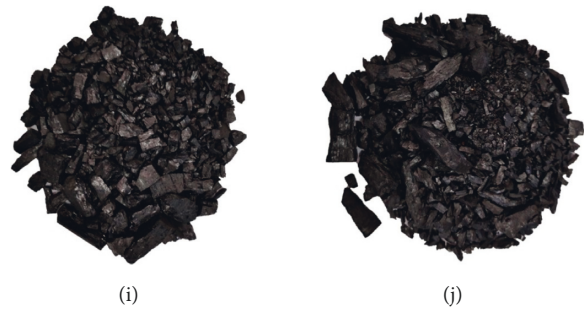

Figure 8: Failure modes of the specimens under uniaxial compression at different impact pressures. (a) $P = 0.13$ MPa. (b) $P = 0.17$ MPa. (c) $P = 0.25$ MPa. (d) $P = 0.30$ MPa. (e) $P = 0.50$ MPa. (f) $P = 0.70$ MPa. (g) $P = 0.90$ MPa. (h) $P = 1.20$ MPa. (i) $P = 1.50$ MPa. (j) $P = 2.00$ MPa.

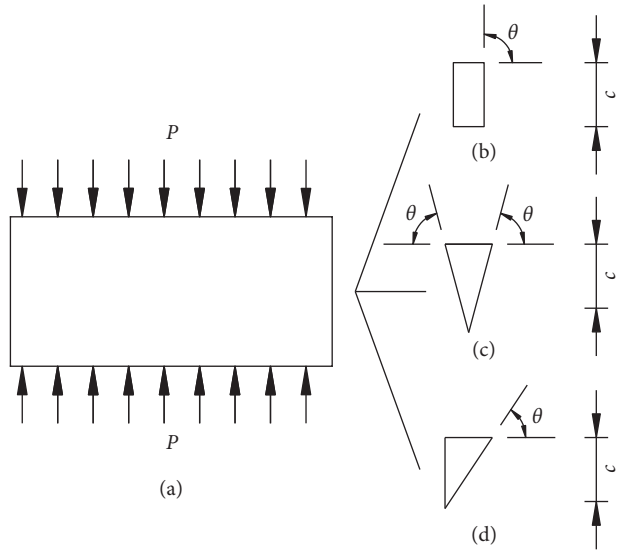

Figure 9: Fragmentation patterns of the coal specimens under impact loading. (a) Specimen loading mode, (b) splitting rectangular section fragment, (c) conical section fragment, and (d) wedge section fragment.

(m_{iv}) is obtained by using the mass of each group of the particle size fragments (m_{di}) and the mass of the original coal specimen (m). Third, by multiplying the mass percentage of each group of the particle size fragments (m_{iv}) by the average particle size of the group (d_{iv}), the proportion of the particle size of the group in all the groups (δ_{iv}) is obtained. Finally, the average particle size of the coal specimen under a certain impact pressure (δ) is obtained by superimposing the percentage of the particle size of each group:

$$\delta = \sum_{1}^{i} \delta_{iv} = \sum_{1}^{i} m_{iv} d_{iv}, \tag{2}$$

where i is the sieving grade group and d_{iv} is the average particle size of each group, that is, the average of the maximum particle size and the minimum particle size of the i group. For example, when $i = 1$, the average particle size is 32.5 mm.

Through sieving and calculation, the mass percentage and average particle size of the fragments at various strain rates are obtained. As shown in Table 1, m is the original mass of the specimen and m_{iv} is the mass percentage of group i. Figure 12 shows the particle-size distribution characteristics and the dynamic characteristics of the average particle size with impact pressure.

From Table 1 and Figure 12, the fragmentation distribution and average particle size of coal specimens under different impact pressures have a significant impact.

Specifically, during the process of increasing the pressure from 0.13 MPa to 2.00 MPa, the mass percentage of fragments in the maximum particle size group (15.0–50 mm) decreased gradually from 98.93% to 4.65%, and the decrease was 95.30%. The mass of the fragments in the following three groups (10.0–15.0 mm, 5.0–10.0 mm, and 2.0–5.0 mm) showed the characteristics of first increasing and then decreasing. The maximum percentages of the fragments in the three groups were 35.43%, 32.11%, and 21.30%. The mass percentages of the smallest two groups (1.0–2.0 mm and 0.0–2.0 mm) increased rapidly with increasing air pressure from 0.13 MPa to 2.00 MPa, from 0.07% to 23.33% in the range of 1.0–2.0 mm and from 0.05% to 9.45% in the range of 0–1.0 mm.

Overall, the average particle size decreases with increasing air pressure, which indicates that the damage degree of the specimen increases gradually. The change in the average particle size can be roughly divided into three processes: increasing pressure from 0.13 to 0.30 MPa, and a rapidly decreasing average particle size from 32.21 mm to 19.64 mm (a decrease of 39.03%); increasing pressure from 0.30 MPa to 0.90 MPa, and a slow decrease in the average particle size from 19.64 mm to 12.54 mm (a decrease of 36.15%). When the pressure increases further, the average particle size decreases from 12.54 mm to 7.34 mm (a decrease of 41.47%).

3.4. Fractal Dimension Characteristics of the Fragmentation of the Specimens. The fractal dimension can be used to quantitatively describe the degree of coal specimen breakage in the SHPB test to more accurately describe the change rule of the coal specimen breakage degree with impact pressure. The fractal dimension is positively correlated with the damage degree of the specimens; that is, if the damage degree of the specimens increases, then the calculated fractal dimension also increases. At present, the fractal dimension is calculated by mass-equivalent size. The calculation formulas are as follows:

Figure 10: Fragment size grading sieves after impact crushing.

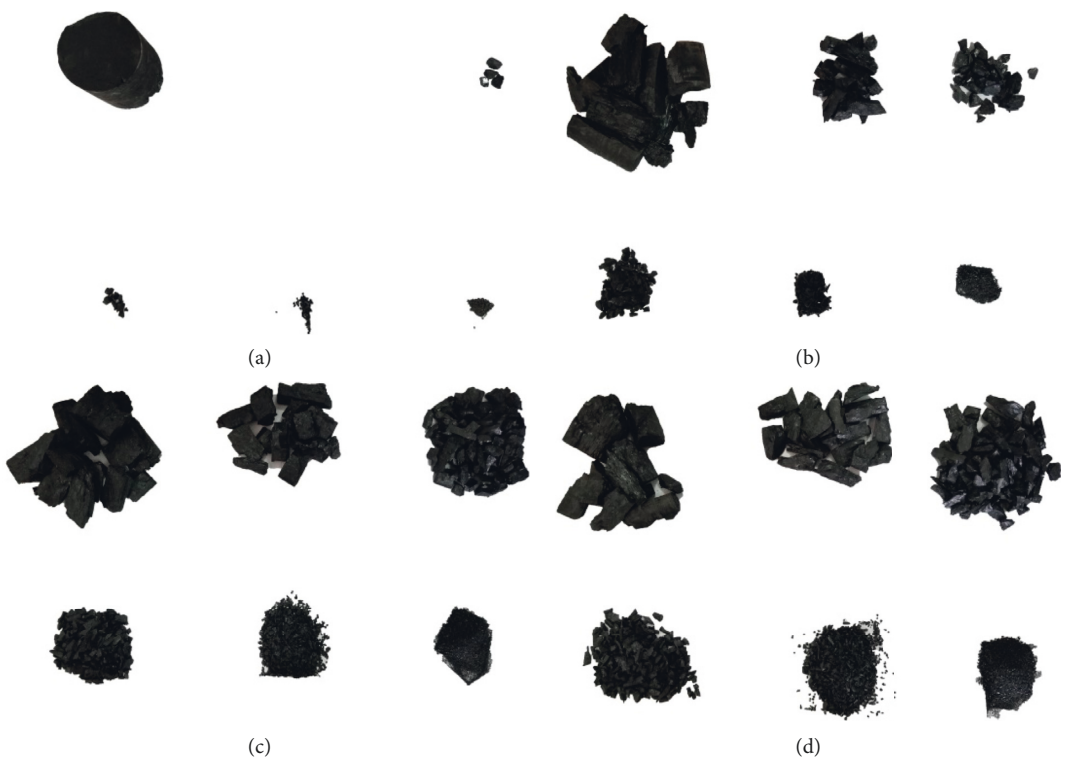

Figure 11: Continued.

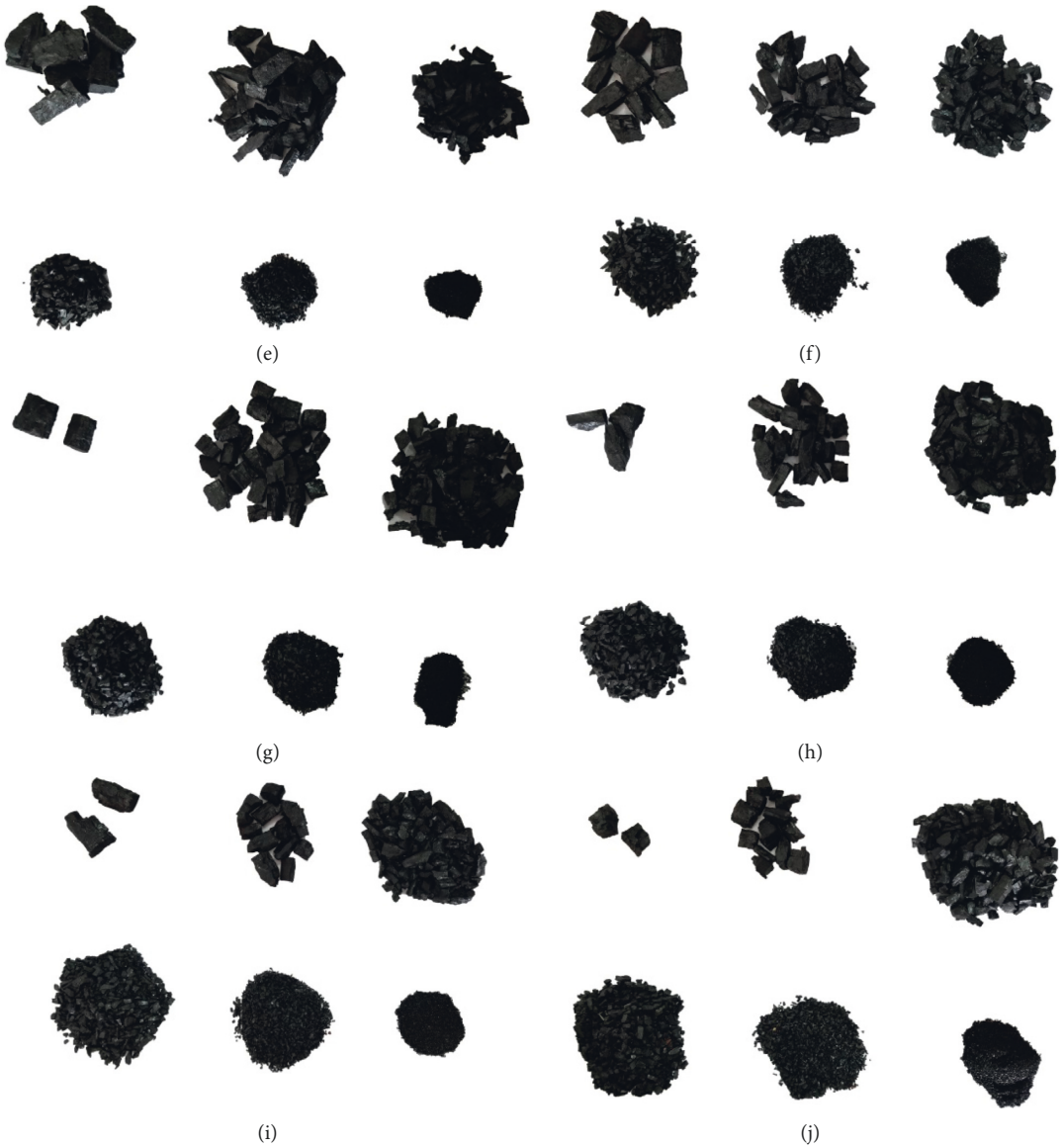

Figure 11: Characteristics of the coal specimen fragments under different pressure impacts. (a) $P = 0.13$ MPa. (b) $P = 0.17$ MPa. (c) $P = 0.25$ MPa. (d) $P = 0.30$ MPa. (e) $P = 0.50$ MPa. (f) $P = 0.70$ MPa. (g) $P = 0.90$ MPa. (h) $P = 1.20$ MPa. (i) $P = 1.50$ MPa. (j) $P = 2.00$ MPa.

Table 1: Distribution characteristics of the fragmentation of coal specimens at different pressures.

P/MPa	m (g)	m_{iv} (%)						Δ (mm)
		$i = 1$	$i = 2$	$i = 3$	$i = 4$	$i = 5$	$i = 6$	
0.13	119.70	98.93	0.00	0.68	0.27	0.07	0.05	32.21
0.17	118.80	74.98	15.52	6.12	2.1	0.81	0.47	27.63
0.25	122.30	49.99	24.09	14.51	6.13	3.69	1.59	21.83
0.30	118.20	37.14	34.98	15.16	6.84	4.22	1.66	19.64
0.50	120.80	32.52	30.12	21.15	9.02	4.98	2.21	17.83
0.70	121.80	30.25	25.26	26.02	11.87	4.79	1.81	16.70
0.90	121.80	10.27	35.43	31.23	15.65	6.47	2.95	12.54
1.20	120.10	9.07	23.33	30.07	20.32	14.14	3.07	10.22
1.50	127.50	10.3	15.99	32.11	21.37	15.71	4.52	9.56
2.00	132.30	4.65	14.68	29.63	18.26	23.33	9.45	7.34

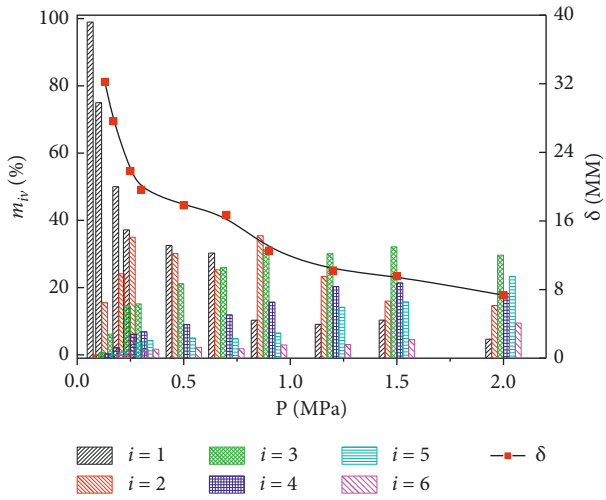

Figure 12: Distribution of the particle size and variation in the average particle size with impact pressure.

$$D = 3 - d, \tag{3}$$

$$d = \frac{\lg(M_R/M)}{\lg R}, \tag{4}$$

where D is the fractal dimension of the fragments; d is the slope of the line drawn in logarithmic coordinates; M_R is the cumulative mass of the fragments smaller than R in diameter; and M is the original mass of the specimen.

According to the cumulative mass and original mass of the specimen in Table 2, the straight lines under different impact pressures ($\lg(M_R/M) - \lg R$) can be drawn according to formula (3). As shown in Figure 13, the slope d of each relation line can be calculated. The fractal dimension D of fragments after coal specimen failure can be obtained by substituting the slope d value into formula (4).

Figure 14 shows the change curve of the fractal dimension of fragments with impact pressure after the failure of the coal specimen. The graph shows that the fractal dimension D of coal increases logarithmically with increasing impact pressure. When the impact pressure increases from 0.15 MPa to 2.00 MPa, the fractal dimension D increases from 1.22 to 2.42, an increase of 98.36%. Because the fractal dimension is positively correlated with the degree of coal fragmentation, it can be concluded that the degree of coal fragmentation increases gradually with increasing impact pressure. The fractal dimension decreases gradually with increasing pressure at higher impact pressures. It can be inferred that the damage degree of the coal specimen increases with increasing impact pressure, but it does not increase infinitely and eventually tends to be stable.

3.5. Distribution Characteristics of Blasting Impact Fragmentation in Open-Pit Mines. To further combine the test results with open-pit coal seam blasting, the size distribution of coal specimen damage under indoor impact load is further divided. After coal seam blasting, especially large coal blocks need to be broken twice, and this greatly increases the cost. Small coal blocks exist in the form of fine particles, which causes serious dust pollution to the mine. These fine particles also increase the cost of dust removal. Therefore, the smaller the proportion of extralarge and small coal blocks after coal seam blasting is, the more effective the control of mining cost is. To further analyze the impact damage effect, the blasting particle size is divided, and the impact effect is evaluated according to the mass percentage of the fragments of the different sizes.

According to the characteristics of the fragmentation distribution of coal specimens under impact load and the requirement of minimum cost control in open-pit coal seam blasting, the fragments are divided into three groups according to the size range: large diameter, medium diameter, and powder. The corresponding particle size ranges of the three groups of fragments are as follows:

(1) Large-diameter fragments: diameter ($d \geq 15.0$ mm), $i = 1$ group of the fragments. This group of fragments has a large scale, which corresponds to a large volume of coal blocks that need secondary blasting after coal seam blasting. Taking the Haerwusu open-pit coal mine as an example, the diameter of the coal block is basically 300 mm on this scale.

(2) Medium-diameter fragments: diameter (15.0 mm $\geq d \geq$ 2.0 mm), $i = 2, 3, 4$ groups of the fragments. The scale of the fragments is moderate. Corresponding with the size of the fragments after coal seam blasting, the fragments in this range do not need to be broken twice. In the Haerwusu open-pit coal mine, the diameter range of the coal blocks in this scale is approximately 150–300 mm.

(3) Powder fragments: diameter ($d \leq 2.0$ mm), $i = 5, 6$ groups of the fragments in the particle size range. The size of the fragments is small, which corresponds to the small volume of coal after blasting, even powder coal. With this size, the economic value of the coal block is small, and for ultrasmall powder coal, the final formation of mine blasting dust.

According to the above method, the distribution characteristics of the fragments with different sizes under different loading pressures can be obtained, as shown in Table 3. Figure 15 shows the variation in the mass percentage of the three groups of coal fragments with air pressure.

As shown in Figure 15, with increasing air pressure, the mass percentage of the fragments varies significantly. Specifically, with increasing air pressure, the mass percentage of large-diameter fragments decreases gradually. The air pressure increases from 0.13 MPa to 2.00 MPa, and the mass percentage of large-diameter fragments decreases from 98.93% to 4.65%, with a range of 95.30%. From the whole process, the air pressure increases from 0.13 MPa to 0.30 MPa, and the mass percentage of large-diameter fragments decreases rapidly in a linear form, with a range of 61.79%. When the air pressure increases from 0.30 MPa to 0.70 MPa, the decreasing trend of the mass percentage of

Table 2: Cumulative mass and fractal dimension of the coal specimen fragments under different pressures.

p (MPa)	Original mass M (g)	Cumulative mass M_R (g)						Slope d	Fractal dimension D
		0–1.0 mm	0.0–2.0 mm	0.0–5.0 mm	0.0–10.0 mm	0.0–15.0 mm	0.0–50.0 mm		
0.13	119.7	0.05	0.12	0.39	1.07	1.07	100	1.78	1.22
0.17	118.8	0.47	1.28	3.38	9.5	25.02	100	1.39	1.61
0.25	122.3	1.59	5.28	11.41	25.92	50.01	100	1.06	1.94
0.30	118.2	1.66	5.88	12.72	27.88	62.86	100	1.06	1.94
0.50	120.8	2.21	7.19	16.21	37.36	67.48	100	0.99	2.01
0.70	121.8	1.81	6.6	18.47	44.49	69.75	100	1.05	1.95
0.90	121.8	2.95	9.42	25.07	56.3	89.73	100	0.94	2.06
1.20	120.1	3.07	17.21	37.53	67.6	90.93	100	0.86	2.14
1.50	127.5	4.52	20.23	41.6	73.71	89.7	100	0.77	2.23
2.00	132.3	9.45	32.78	51.04	80.67	95.35	100	0.58	2.42

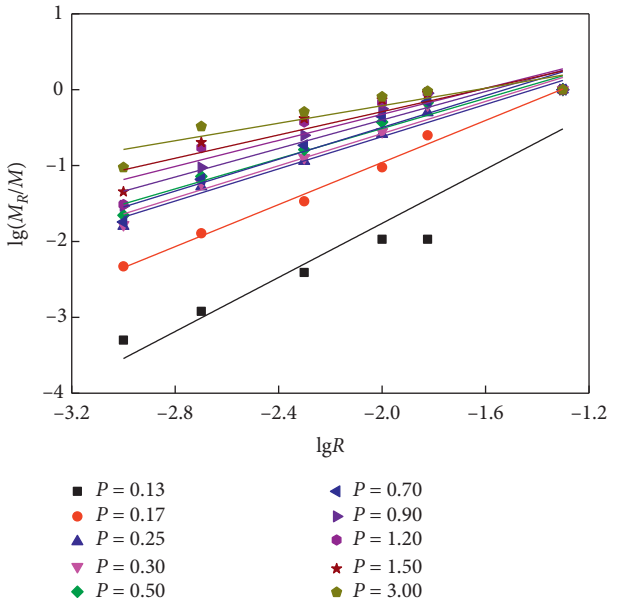

Figure 13: $\lg(M_R/M) - \lg R$ curves at different impulse pressures.

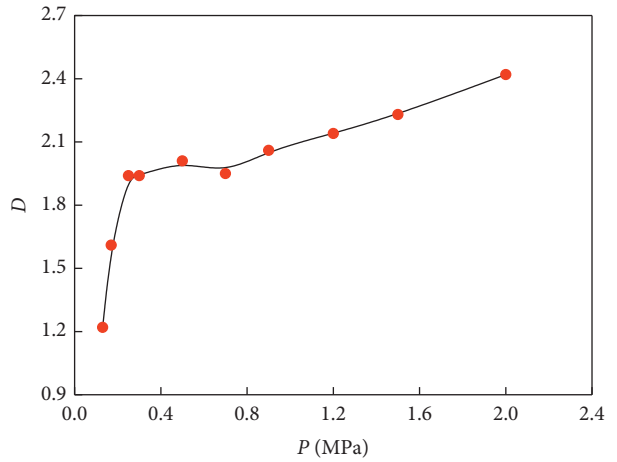

Figure 14: Plot of the fractal dimension versus impact pressure.

large-diameter fragments slows down to 6.89%. However, when the air pressure exceeds 1.20 MPa, the mass percentage of large-diameter fragments remains within 10%.

For medium-diameter fragments, the mass percentage of fragments increases with increasing air pressure, which can be divided into three stages. First, when the pressure increases from 0.13 MPa to 0.30 MPa, the mass percentage of medium-diameter fragments increases rapidly in a straight line form 0.95% to 56.98%, with an increase of 56.03%. When the air pressure increases from 0.3 MPa to 0.9 MPa, the mass percentage of medium-diameter fragments increases slowly from 56.98% to 82.31%, and the increment is 25.33%. When the air pressure exceeds 0.90 MPa, the mass percentage of the fragments decreases and the decrease range is approximately 20%.

Compared with the other two groups, the mass percentage of the powder fragments increases linearly with air pressure. When the air pressure increases from 0.13 MPa to 2.0 MPa, the mass percentage of powder fragments increases from 0.12% to 32.78%, and the increment is 32.66%.

4. Conclusion

Through the above analysis, it can be concluded that increasing the impact pressure can effectively reduce the mass percentage of large-diameter fragments, thus reducing the amount of secondary coal fragments and controlling the input cost of secondary crushing. However, with increasing air pressure, the mass percentage of powder fragments increases gradually, which will greatly increase the cost of dust control in coal mines. Based on these two aspects, two principles of blasting effect evaluation are given.

(1) The mass percentage of medium-diameter fragments is more than 50%. This finding ensures that more than 50% of the coal seam after blasting goes directly into the next stage of the coal preparation process without secondary crushing.

(2) The mass percentage of powder fragments should be less than 10%. Compared with the cost of coal mining in an open-pit coal mine, the cost of dust control (including economic cost and time cost) is much larger. Therefore, the final effect of blasting requires that dust pollution in pits be reduced as much as possible. Thus, the percentage of powder fragment mass should be controlled within a reasonable range of 10%.

Table 3: Size distribution characteristics of the coal blocks under different impact pressures.

Fragment scale	Percentage of mass of coal fragments m_{iv} under each pressure P (MPa)									
	0.13	0.17	0.25	0.30	0.50	0.70	0.90	1.20	1.50	2.00
Large	98.93	74.98	49.99	37.14	32.52	30.25	10.27	9.07	10.30	4.65
Medium	0.95	23.74	44.73	56.98	60.29	63.15	82.31	73.72	69.47	62.57
Powder	0.12	1.28	5.28	5.88	7.19	6.60	9.42	17.21	20.23	32.78

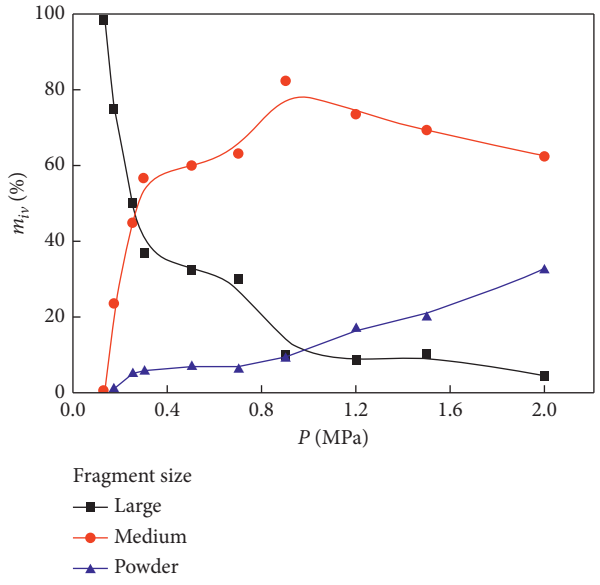

Figure 15: The variation in the mass percentage of three groups of coal fragments with air pressure.

Based on the above two principles, this evaluation can be given by comparing the size distribution characteristics of the fragments under different impact pressures:

(1) The percentage of mass of medium-diameter fragments under an impact load with a pressure less than 0.30 MPa is less than 50%. Therefore, the impact crushing effect is poor in this pressure range.

(2) The percentage of powder fragments under an impact load with a pressure greater than 0.90 MPa is more than 10%. Therefore, the impact fragmentation effect is poor in this range of pressure.

The particle-size distribution of the fragments under impact loading satisfies two principles in the range of loading pressure from 0.30 MPa $\leq P <$ 0.90 MPa and the coal impact crushing effect is satisfactory in this range. However, when the pressure is 0.90 MPa, the mass percentage of powder fragments is 9.42%, close to 10%. Therefore, the pressure is excluded from the good blasting pressure range. Finally, according to the test results and two evaluation principles, the range of pressure with good impact effect in this test is 0.30 MPa $\leq P <$ 0.90 MPa.

Data Availability

The data used to support the findings of this study are available from the corresponding author upon request.

Conflicts of Interest

The authors declare that there are no conflicts of interest regarding the publication of this article.

Acknowledgments

This study was supported by the National Natural Science Foundation of China (Grant nos. 51804299 and 51574222) and the Natural Science Foundation of Jiangsu Province, China (Grant no. BK20180646).

References

[1] C. Qi, X. Tang, X. Dong, Q. Chen, A. Fourie, and E. Liu, "Towards intelligent mining for backfill: a genetic programming-based method for strength forecasting of cemented paste backfill," *Minerals Engineering*, vol. 133, pp. 69–79, 2019.

[2] C. Qi, A. Fourie, Q. Chen, and P. Liu, "Application of first-principles theory in ferrite phases of cemented paste backfill," *Minerals Engineering*, vol. 133, pp. 47–51, 2019.

[3] C. C. Qi, L. Liu, J. Y. He, Q. S. Chen, L. J. Yu, and P. F. Liu, "Understanding cement hydration of cemented paste backfill: DFT study on water adsorption at tricalcium silicate (111) surface," *Minerals*, vol. 9, no. 4, p. 202, 2019.

[4] B. Y. Mao, S. L. Xie, M. L. Xu, X. N. Zhang, and G. H. Zhang, "Simulated and experimental studies on identification of impact load with the transient statistical energy analysis method," *Mechanical Systems and Signal Processing*, vol. 46, no. 2, pp. 307–324, 2014.

[5] H. Qu, "Influence of axial load level on performance of resist impact on tubular T-joint," *Applied Mechanics and Materials*, vol. 166–169, pp. 310–313, 2012.

[6] B. Mao, S. Xie, and X. Zhang, "Identification of impact load using transient statistical energy analysis method," *International Journal of Applied Electromagnetics and Mechanics*, vol. 45, no. 1–4, pp. 353–361, 2014.

[7] Z.-H. Ji and D.-Y. Wang, "Influence of load shape on dynamic response of cross-stiffened deck subjected to in-plane impact," *Thin-Walled Structures*, vol. 82, pp. 212–220, 2014.

[8] M. M. Shokrieh and A. Askari, "Similitude study of impacted composite laminates under buckling loading," *Journal of Engineering Mechanics*, vol. 139, no. 10, pp. 1334–1340, 2013.

[9] A. Vaitkus, V. Vorobjovas, J. Gražulytė, and A. Tumavičė, "Performance of pavements affected by static and impact load," *Applied Mechanics and Materials*, vol. 614, pp. 627–630, 2014.

[10] H. B. Chu, X. L. Yang, W. M. Liang, Y. Q. Yu, and L. P. Wang, "Experimental study on the blast damage law of the simulated coal," *Journal of Mining & Safety Engineering*, vol. 28, no. 3, pp. 488–492, 2011.

[11] H. Chu, W. Liang, Y. Yu, and X. Yang, "Simulation experiment study on the coal blast damage and failure," in *Rock*

Mechanics: Achievements and Ambitions, pp. 771–774, Taylor and Francis Group, London, UK, 2012.

[12] W. C. Zhu, C. H. Wei, S. Li, J. Wei, and M. S. Zhang, "Numerical modeling on destress blasting in coal seam for enhancing gas drainage," *International Journal of Rock Mechanics and Mining Sciences*, vol. 59, pp. 179–190, 2013.

[13] D. S. Preece and S. H. Chung, "Modeling coal seam damage in cast blasting," in *Proceedings of the Twenty-Fifth Annual Conference on Explosives and Blasting Technique*, pp. 233–240, Nashville, TN, USA, February 1999.

[14] S. R. Wang, H. H. Jia, and M. S. Chang, "Analysis of accumulated damage effects on the roof of mined-out areas under blasting vibration," *Advanced Building Materials*, vol. 250–253, no. 1–4, pp. 2346–2351, 2011.

[15] P. C. Xu, Q. Dong, X. P. Li, and Y. Luo, "Influence research of underground caverns blasting excavation on excavation damage zone of adjacent cavern," *Advanced Materials Research*, vol. 838–841, pp. 901–906, 2013.

[16] D. Zhang, S. Yao, F. Lu et al., "Experimental study on scaling of RC beams under close-in blast loading," *Engineering Failure Analysis*, vol. 33, pp. 497–504, 2013.

[17] X. Xue, X. Yang, and W. Zhang, "Numerical modeling of arch dam under blast loading," *Journal of Vibration and Control*, vol. 20, no. 2, pp. 256–265, 2014.

[18] L. Liu, M. Chen, W. B. Lu, Y. G. Hu, and Z. D. Leng, "Effect of the location of the detonation initiation point for bench blasting," *Shock and Vibration*, vol. 2015, Article ID 907310, 11 pages, 2015.

[19] E. A. Chi and Y. P. Zhang, "Harmfulness and control measures of air shock-wave induced by building demolition blasting," *Progress in Safety Science and Technology*, vol. 8, pp. 1113–1117, 2010.

[20] T. Wang, W. L. Yu, S. Q. Dong, W. Quan, and M. Ma, "Blast effects of spherical explosive charge in soil-concrete multi layer medium," *Theory and Practice of Energetic Materials*, vol. 8, pp. 498–502, 2009.

[21] S. Wang, L. Shen, G. D. Nguyen, F. Maggi, A. El-Zein, and Y. Zheng, "An empirical approach for the quantification of uniaxial compressive stress-strain of partially saturated granular media under high strain rates," *Soil Dynamics and Earthquake Engineering*, vol. 120, no. 5, pp. 245–256, 2019.

[22] I. T. Wang, "Numerical simulation and experimental validation of the mach reflection effect of shock wave under ground surface blast," *Journal of Vibroengineering*, vol. 17, no. 3, pp. 1413–1423, 2015.

[23] S. Wang, E. A. Flores-Johnson, and L. Shen, "A technique for the elimination of stress waves overlapping in the split Hopkinson pressure bar," *Experimental Techniques*, vol. 41, no. 4, pp. 345–355, 2017.

[24] J. E. Field, S. M. Walley, W. G. Proud, H. T. Goldrein, and C. R. Siviour, "Review of experimental techniques for high rate deformation and shock studies," *International Journal of Impact Engineering*, vol. 30, no. 7, pp. 725–775, 2004.